catalysts

MDPI

Article

A Facile Synthesis of $Bi_2O_3/CoFe_2O_4$ Nanocomposite with Improved Synergistic Photocatalytic Potential for Dye Degradation

Abdul Basit Naveed, Fakhira Riaz, Azhar Mahmood *, Ammara Shahid and Saman Aqeel

School of Natural Sciences, National University of Sciences and Technology, H-12, Islamabad 44000, Pakistan; baasitlali@gmail.com (A.B.N.); fakhirariaz22@gmail.com (F.R.); ammarashahid04@gmail.com (A.S.); samanaqeel8910@gmail.com (S.A.)

* Correspondence: dr.azhar@sns.nust.edu.pk; Tel.: +92-51-9085-5574

Abstract: Semiconductor-based photocatalysis is a probable approach to overcoming many pollution problems and eradicating toxic organic materials from wastewater. This research endeavor aimed to explore the synergistic potential of different semiconductor nanocomposites for photocatalytic degradation of organic pollutants in contaminated water. A facile hydrothermal approach was employed to synthesize bismuth oxide and cobalt ferrite nanoparticles from their precursors—bismuth nitrate pentahydrate, ferric chloride hexahydrate and cobalt chloride hexahydrate—with various concentrations and conditions to optimize the product. Subsequently, nanocomposites of bismuth oxide and cobalt ferrite were prepared by solid-state mixing in varying concentrations followed by calcination. UV/visible diffuse reflectance spectroscopy, X-ray diffraction, scanning electron microscopy and elemental dispersive X-ray spectroscopic techniques have corroborated the successful synthesis of nanocomposites. The energy gaps of bismuth oxide and cobalt ferrite nanocomposites were computed in the range of 1.58–1.62 eV by Tauc plots. These nanocomposite materials were ascertained for photocatalytic potential to degrade methyl orange organic dye in water. A nanocomposite with equiquantic proportions has shown the best photocatalytic degradation activity, which may be attributed to the type-II band configuration and a synergistic effect, because Bi_2O_3 acts as an electron sink. This synergism has reduced the cogent band gap, hindered electron hole recombination and increased electron hole availabilities for photodegradation reactions, thus ensuing an efficient photodegradation co-work of $Bi_2O_3/CoFe_2O_4$ nanocomposites.

Keywords: photocatalyst; nanocomposite; energy gap; dye degradation; hydrothermal synthesis

Citation: Naveed, A.B.; Riaz, F.; Mahmood, A.; Shahid, A.; Aqeel, S. A Facile Synthesis of $Bi_2O_3/CoFe_2O_4$ Nanocomposite with Improved Synergistic Photocatalytic Potential for Dye Degradation. *Catalysts* **2021**, *11*, 1180. https://doi.org/10.3390/catal11101180

Academic Editors: Jaime Carbajo and Patricia García-Muñoz

Received: 6 June 2021
Accepted: 24 August 2021
Published: 28 September 2021

1. Introduction

Water pollution is a major environmental problem worldwide. Wastewater contains numerous hazardous and toxic substances such as dyes, resins, heavy metals, phenolic compounds, pesticides and herbicides etc. [1–3]. Dye pollutants are carcinogenic and mutagenic; they can lead to central nervous system dysfunction and may cause morbidity in human as well as in aquatic life [4,5]. Conventional wastewater treatment pathways are not effective because of the contumacious nature of synthetic dyes and the high salinity of wastewater [6,7]. Ozonation and chlorination are also quite incapable because of their high operating costs [8,9]. The conventional physical methods, such as adsorption via activated carbon, ion exchange through synthetic adsorbent resins, reverse osmosis, ultrafiltration, coagulation by chemical agents etc., have been employed for the removal of toxic dyes from water [10,11]. These procedures are successful for transferring organic pollutants from water to another form, thereby producing secondary pollution which needs more treatment for removal of solid wastes and regeneration of the adsorbent and, thus, raises the cost of the process [12–14]. Among these contaminants, dyes, phenolics and pesticides have been of major concern because of their harmfulness to the environment. Advanced

oxidation processes have potential for the removal of water polluted with hard degradable organic compounds. Moreover, hybrid processes combining membrane separation and heterogeneous photocatalysis, called photocatalytic membrane reactors, offer an amazing solution by complementing the advantages and overcoming the challenges of each other.

Photocatalytic oxidation involves advanced oxidation techniques for the degradation of dyes and many other toxic organic pollutants [15–17]. Nowadays, semiconductors are used as photocatalysts as they are cost-effective and have furnished good results. The most effective photocatalysts found in the literature are selenides, sulfides, metal oxides and the compounds with a modest band gap energy of 1.1–3.8 eV, such as TiO_2, ZnO and WO_3. However, these metal sulfides and selenides have issues, such as instability, photo anodic corrosion and toxicity [18–22].

Recently, cobalt ferrite has hugely attracted researchers for its utilization in photocatalytic wastewater treatment [23–29]. $CoFe_2O_4$ and its composites are low-cost and possess extraordinary magnetic properties, which results in higher adsorption ability as compared to other photocatalysts. Their photocatalytic activity improves owing to their narrow band gap, rapid transfer capability for charge carriers, higher visible light response, chemical functionalities, morphologies and annealing temperature. Dutta et al. reviewed the photocatalytic activity of $CoFe_2O_4$ against noxious organic pollutants in water and pointed out its limitations, such as aggregation, the recombination rate of electron holes and photocorrosion [25]. Their study concluded that the formation of $CoFe_2O_4$-based heterojunctions is seemingly acceptable for the improved photocatalytic performance, because the combination of $CoFe_2O_4$ with other photocatalysts that have various band gap positions would exhibit synergistic effects, which permits more pollutant compounds to be accessible for photodegradation and enhances the rate of charge separation, thus reducing electron hole recombination. Habibi and Parhizkar prepared spinel phase $CoFe_2O_4$ nanocomposites through a hydrothermal method using $CoFe_2O_4$ and iron nitrate as precursors and ethylene glycol as a chelating agent [26]. Their product has demonstrated an energy gap of 1.3 eV and 68.0% breakdown of Reactive Red 4 (azo dye) within 100 min. They mainly attribute this enhanced activity to the shift of electrons and holes to the surface of nanocomposites, which hinders electron hole recombination. Cubic ferro spinel nanostructures of $Co_{0.2}Zn_{0.8}Fe_2O_4$ were prepared by A. Boudjemaa et al. via coprecipitation [23]. These structures were n-type semiconductors with a lower band gap which dramatically enhanced photocatalytic activity under visible light irradiation. Z. Yamani studied photocatalytic degradation performance of magnetically separable $CoFe_2O_4$/BiOCl composites against Rhodamine B under UV light irradiation [29]. Yamani concluded that the adsorption of RhB molecules was favored on the surface, caused by the development of heterojunctions on the interface between BiOCl and ferrites. Y. Deng et al. successfully synthesized a recyclable photo-Fenton catalyst, of composition $CoFe_2O_4$@polypyrrole, by simple in situ Fenton oxidization polymerization [24]. This catalyst system has exhibited 90% discoloration in up to five cycles against methyl orange, methylene blue and rhodamine B. The degradation measurement in the presence of reactive species scavengers has revealed that the holes and the hydroxyl radical were the major reactive oxygen species in the $CoFe_2O_4$@PPy system. Y. Deng et al. has attributed this performance enhancement to the combination of enhanced Fenton response by coordinated PPy and Fe^{2+} redox pairs and photocatalytic performance by improved photo-led charge separation and adsorption. A boost in catalytic performance of pristine $CoFe_2O_4$ was observed by R. Sharma when yttrium was doped into a cobalt ferrite single-phase cubic spinel structure [27]. This increased BET surface area values and a reduced band gap. The good recyclability of prepared photocatalysts has proven the good stability of the materials used in wastewater treatment. A $CoFe_2O_4$/PMS (peroxymonosulphate) system, prepared by sol-gel combustion method, has demonstrated good photodegradation of methyl orange and phenol [28]. Surface hydroxyls of Co^{2+}/PMS have played a significant role in the generation of sulphate and hydroxyl free radicals in neutral medium, producing more surface active sites.

Among numerous semiconductors, Bi_2O_3 and $CoFe_2O_4$ are potent candidates for photoactive nanocomposite preparations due to their distinctive structures and physical aspects, such as band gap, thermal stability, high oxygen ion conductivity and high refractive index. However, bare Bi_2O_3 and $CoFe_2O_4$ show less photo catalytic activity, owing to photo corrosion, rapid charge carrier recombination and structural conversions [30–33]. Different methods can be utilized to increase the photocatalytic activity of Bi_2O_3 and $CoFe_2O_4$, such as doping of transition metal oxides or rare earth metals and formation of nanocomposites in order to sensitize the photocatalyst to photo energy and to keep electron hole pairs separate. One of the most efficient ways to resolve this issue is to prepare nanocomposites of compatible semiconductor materials with a synergistic effect that will help charge migration [34–47].

The present study has explored the compatibility of Bi_2O_3 and $CoFe_2O_4$ for the preparation of photoactive nanocomposites with good photodegradation potential against methyl orange dye. To our knowledge, no earlier research has been reported in the literature regarding the synthesis of $Bi_2O_3/CoFe_2O_4$ nanocomposites and their dye degradation potential.

2. Results

This study aimed to develop different nanocomposites of bismuth oxide and cobalt ferrite semiconductor materials that work synergistically to improve photocatalytic activity for efficient photodegradation of methyl orange dye. As-prepared nanocomposite materials were characterized by X-ray diffraction (XRD), scanning electron microscopy (SEM) and energy dispersive X-ray (EDX) spectroscopic techniques while their energy gaps were gauged by UV/Vis diffuse reflectance spectroscopy (DRS) via Tauc plots. Photodegradation experiment results were employed to study photocatalytic efficiency.

2.1. Phase Analysis

XRD patterns of prepared samples were scanned in the range of 10° to 70° by X-ray diffractometer (D8 advance, BRUKER, Camarillo, CA, USA) with Cu-Kα radiation (k = 1.5406 Å) at room temperature. All the peaks in Figure 1a were found to be consistent with the available standard JCPDS 01-077-0426 and can be indexed to a single-phase cubic $CoFe_2O_4$ structure. Reflection (220), exhibited at 30.12° exclusively, depends on the Co^{2+} cations occupying the cubic sites. No additional and intermediate phases were observed within the sensitivity of the experimental measurements. The crystallite size of as-prepared $CoFe_2O_4$ particles was computed by the classical Scherrer formula [48]. Dhkl = kλ/βcosθ, where Dhkl is the crystallite size derived from the (311) peak of the XRD spectrum, k the sphere shape factor (0.89), θ the angle of diffraction, β the difference between the full width at half-maximum (FWHM) of the sample peak and the standard SiO_2 used to calibrate the intrinsic width associated with the instruments and λ the X-ray wavelength (1.5406 Å). The obtained crystallite size of as-prepared $CoFe_2O_4$ particles was about 26.6 nm (Table 1). The XRD pattern of Bi_2O_3 (Figure 1e) was in agreement with the available standard JCPDS 00-022-0515. The crystal system of Bi_2O_3 was a tetragonal form which is a metastable two-dimensional superstructure of β-Bi_2O_3 [49]. Diffraction lines of Bi_2O_3 patterns have indicated that the powder has a good degree of crystallinity (Figure 1e). The crystallite size of Bi_2O_3 was computed from the full width at half-maximum intensity of the (201) X-ray line diffraction and was found to be approximately 32 nm.

With the increase in Bi_2O_3 content in $Bi_2O_3/CoFe_2O_4$ nanocomposites, the intensity of the (201) peak at 27.42°, which is identified as the main peak of the Bi_2O_3 phase, gradually increased, whereas that of the (311) peak at 35.16°, inherent from the $CoFe_2O_4$ phase, was decreased. It was evident from Figure 1b–d that individual peaks of Bi_2O_3 and $CoFe_2O_4$ varied directly with their proportions in as-prepared nanocomposite materials, thus depicting no chemical reaction between the constituent chemicals. Furthermore, the purity of the samples is also apparent from the lack of any extra peak in the diffraction patterns of all prepared photocatalysts.

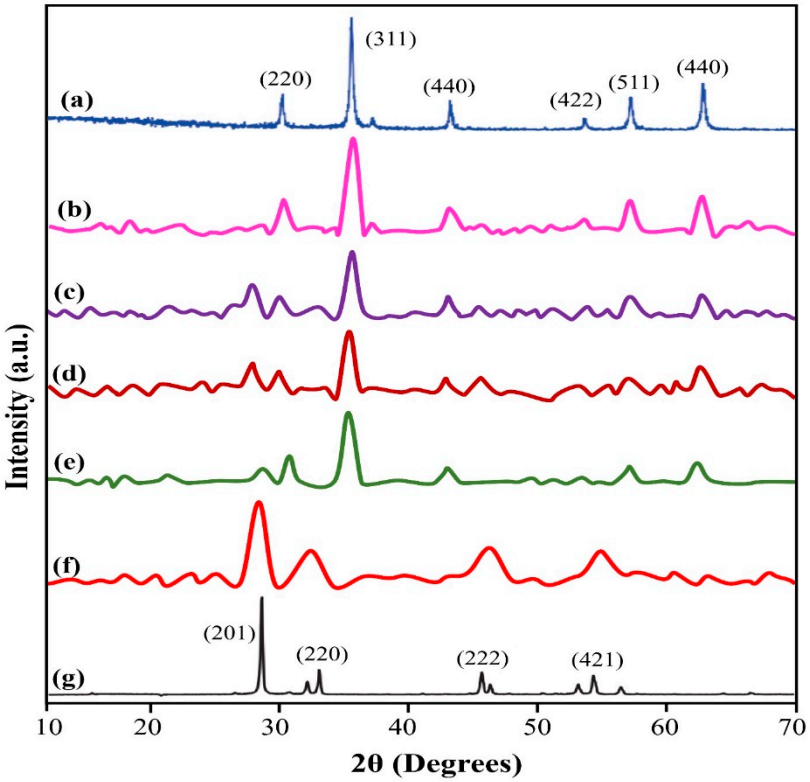

Figure 1. XRD patterns of (**a**) $CoFe_2O_4$ [32]; (**b**) $CoFe_2O_4$ (as-prepared); (**c**) NC-3; (**d**) NC-2; (**e**) NC-1; (**f**) Bi_2O_3 (as-prepared); (**g**) Bi_2O_3 [43].

Table 1. Crystallite size of prepared samples.

Sample	Average Crystallite Size (nm)
Bi_2O_3	32
$CoFe_2O_4$	26.6
NC-1	19
NC-2	21
NC-3	30

2.2. Elemental Analysis

EDX analysis was performed by a VEGA3 machine (TESCAN, Kohoutovice, Czech Republic) to determine the elemental composition of prepared samples. Each element showed its specific peaks in the graph, signifying its quantified presence in the sample. All peaks corresponded to $CoFe_2O_4$ with no extra peak showing the purity of the sample. The spectrum depicted signals of cobalt, iron and oxygen with 17.43%, 30.48% and 52.09% by weight, respectively. The composition, determined by energy-dispersive spectroscopy, showed the stoichiometry of $CoFe_2O_4$. Since the atomic numbers of cobalt and iron are closer, the ratio of the X-ray intensities from these elements generally associated with their composition. The intensity ratio of Co:Fe was about 1:2, as determined by the EDX. In this case, X-ray intensities do not need to be compensated for absorption and fluorescence effects, as these particles are smaller than the free path required for X-ray transmission through solids, i.e., 100 nm. The EDX pattern of Bi_2O_3 has shown no extra peak, which indicates that the sample was pure. The spectrum has shown signals of O and Bi with 23.06% and 76.94% by weight, respectively (Table 2).

Table 2. EDX elemental data of as-prepared samples.

Sample	Elemental Weight Percentage			
	Co	**Fe**	**Bi**	**O**
$CoFe_2O_4$	17.43	30.48	-	52.09
Bi_2O_3	-	-	23.06	76.94
NC-1	21.20	44.19	19.97	14.63
NC-2	13.13	28.14	25.42	33.31
NC-3	10.73	17.74	47.89	23.63

Qualitative and quantitative EDX results from the nanocomposites agreed with as-prepared compositions, which indicates that no element was lost due to any volatile product formation by heating during nanocomposite calcination.

2.3. Morphological Analysis

A field-emission scanning electron microscope (VEGA3 TESCAN) was used for morphological studies of as-prepared Bi_2O_3, $CoFe_2O_4$ and their nanocomposites. SEM micrographs (Figure 2a–e) were recorded at 200 and 500 nm scales to examine the morphology of the prepared materials. The textures of pure $CoFe_2O_4$ and Bi_2O_3 were observed as granular nanoparticles (Figure 2a,b).

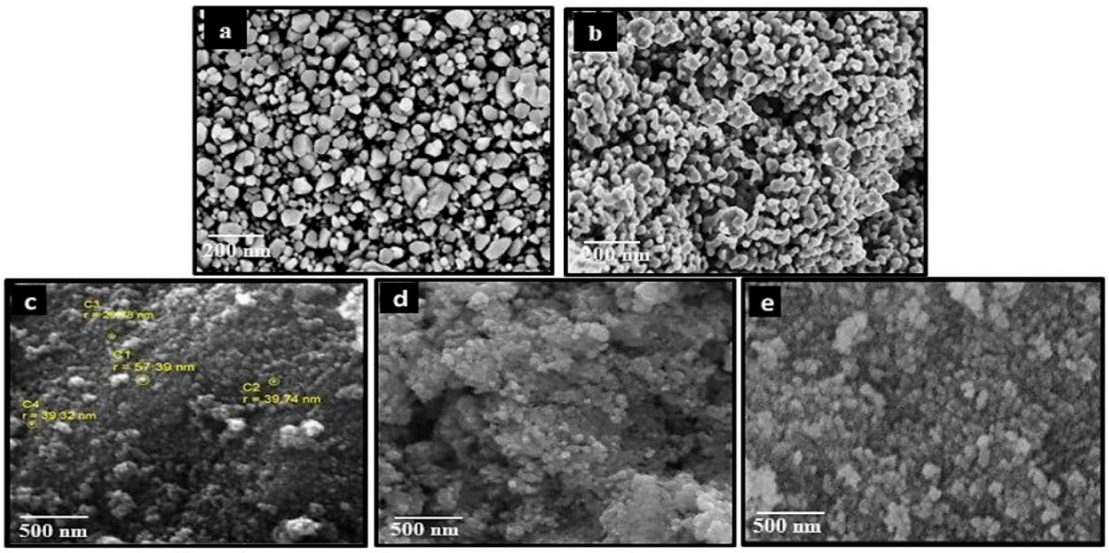

Figure 2. SEM images of (**a**) Bi_2O_3; (**b**) $CoFe_2O_4$; (**c**) NC-1; (**d**) NC-2; (**e**) NC-3.

Scanning electron micrographs of as-prepared nanocomposites have shown irregular granular microstructures with slight agglomeration despite the dipolar interaction between the particles. For compositional uniformity from particle to particle, it was demonstrated that both Bi_2O_3 and $CoFe_2O_4$ phases were positioned on the grain surface side-by-side. Hence, the prepared $Bi_2O_3/CoFe_2O_4$ nanocomposites were considered to be a tightly contacting heterojunction structure between Bi_2O_3 and $CoFe_2O_4$, formed in nano-size level. SEM images of the $Bi_2O_3/CoFe_2O_4$ nanocomposites have shown no significant change in the morphology of the constituent nanoparticles. However, it was established that as Bi_2O_3 contents were increased, the grains in the nanocomposite matrix became larger and more agglomerated, while the shape of the grains was not changed (Figure 2c–e). SEM micrographs have shown that the average particle size of prepared nanoparticles and their composites was below 100 nm, which was also in agreement with those computed from the X-ray powder diffraction peaks.

2.4. Diffuse Reflectance Spectroscopy and Tauc Plots

DRS spectra were employed to construct Tauc plots of the prepared catalysts. Tauc plots were plotted between photon energy and $(\alpha h\nu)^2$ to calculate band gaps. Bi_2O_3 has shown a single hump at 521 nm. Extrapolation of the linear region of the Tauc plot (inset Figure 3a) has furnished a band gap of 2.55 eV for hydrothermally prepared Bi_2O_3. $CoFe_2O_4$ has an intrinsic black color, so it has shown absorption in a wide range of wavelengths [50]. The absorption spectra of cobalt ferrite exhibited a single hump at 751 nm. As cobalt ferrite is a direct semiconductor, the band gap value was 1.63 eV, computed from the Tauc plot (inset Figure 3b). The band gaps of the nanocomposites, namely NC-1, NC-2 and NC-3, were calculated as 1.62, 1.58 and 1.61 eV, respectively, by Tauc plots (inset Figure 3c–e). For the $Bi_2O_3/CoFe_2O_4$ nanocomposites, absorbance reduced as the loading of Bi_2O_3 increased. However, those values of absorbance could be useful in predicting the relative amount of $CoFe_2O_4$ and Bi_2O_3 in the synthesized composites by using the Beer–Lambert law.

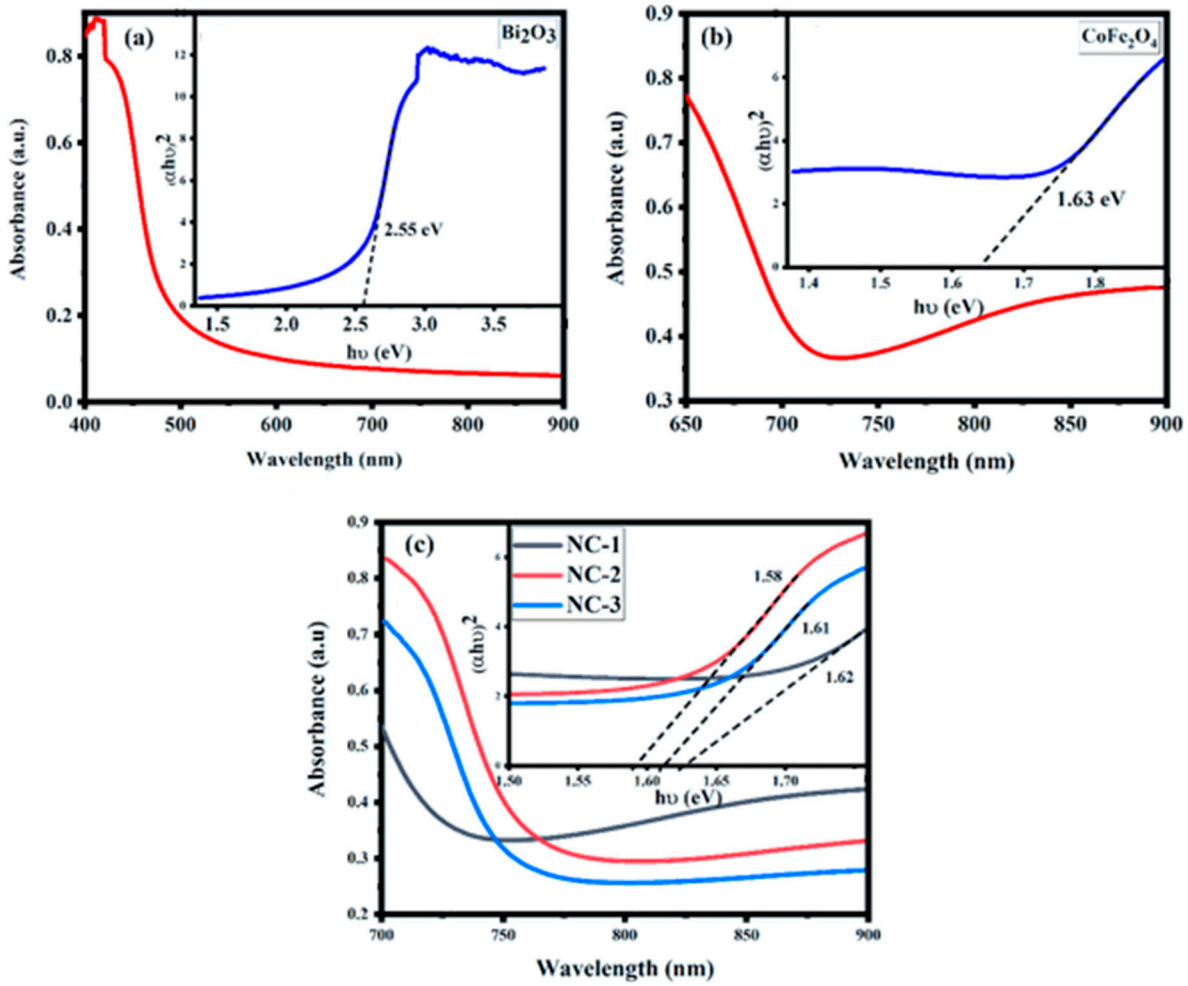

Figure 3. DRS spectra and Tauc plots of (**a**) Bi_2O_3; (**b**) $CoFe_2O_4$; (**c**) NC-1, NC-2, NC-3.

2.5. Photodegradation Activity

The degradation of methyl orange dye was studied by logging changes in the absorption value of a charged dye solution at its $\lambda_{max} \approx 462$ nm for different hourly time intervals of a light irradiation experiment (Table 3). Figure 4 shows degradation spectra of methyl orange for each prepared catalyst along with a blank sample. The photodegradation activities of all prepared nanocatalysts were plotted in terms of percentage degradation versus passage of time (Figure 5). NC-1 (1:3 $Bi_2O_3/CoFe_2O_4$) has also shown good degradation

results. It degraded up to 82% of the dye in 5 h of light exposure. NC-2 (1:1 $Bi_2O_3/CoFe_2O_4$) has shown the best degradation results. It degraded up to 92% of the dye in 5 h of the light irradiation experiment, as evidenced from the associated absorbance spectra taken during photocatalytic bleaching. NC-3 (3:1 $Bi_2O_3/CoFe_2O_4$) has shown moderate degradation results. It degraded up to 78% of the dye in 5 h of light illumination (Figure 6). These results have shown that all prepared nanocomposites exhibited good photodegradation activities as compared to bare materials. The blank with no nanocatalyst has exhibited a minimal decrease, i.e., about 2%, in absorbance when subjected to light irradiation for the period of 5 h witnessed in Figure 4. This shows an evident synergism phenomenon operating between the constituents of the nanocomposites.

Table 3. Absorbance values of dye solutions charged by various as-prepared photocatalysts during photodegradation experiment in comparison to blank.

Sample	**Absorbance**					
Time (h)	0	1	2	3	4	5
MO-Blank	1.00	0.998	0.995	0.991	0.986	0.980
$CoFe_2O_3$	0.99	0.97	0.94	0.86	0.67	0.37
Bi_2O_3	0.95	0.91	0.89	0.82	0.53	0.24
NC-I	0.85	0.79	0.76	0.63	0.32	0.15
NC-II	0.82	0.77	0.74	0.58	0.34	0.06
NC-III	0.88	0.84	0.82	0.67	0.48	0.19

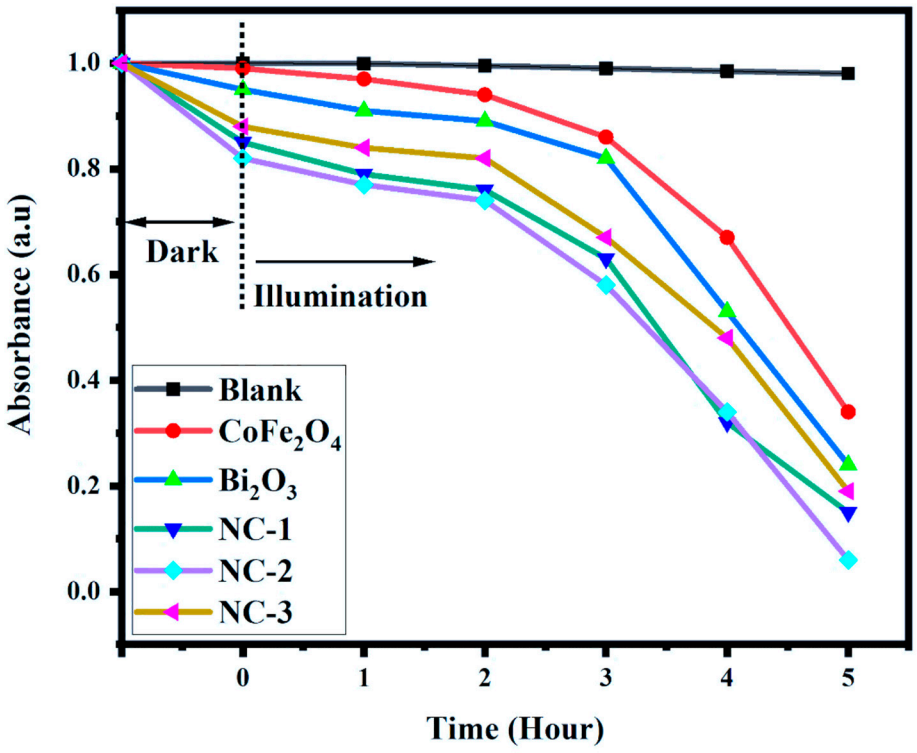

Figure 4. Absorbance of dye solutions charged by various as-prepared photocatalysts during photodegradation experiment.

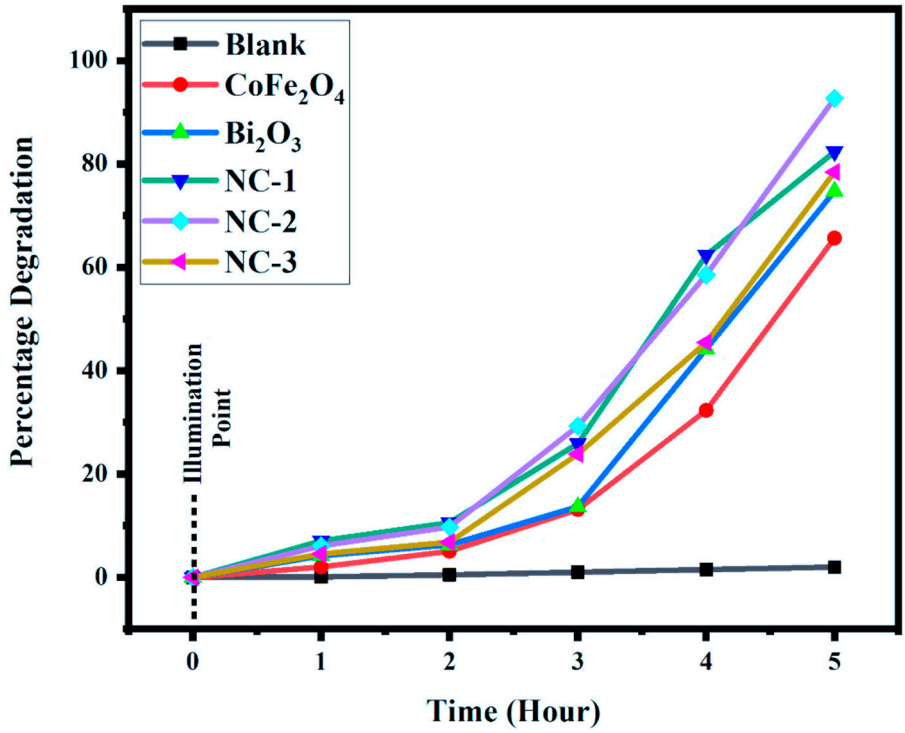

Figure 5. Photodegradation activities of as-prepared photocatalysts against methyl orange dye solution.

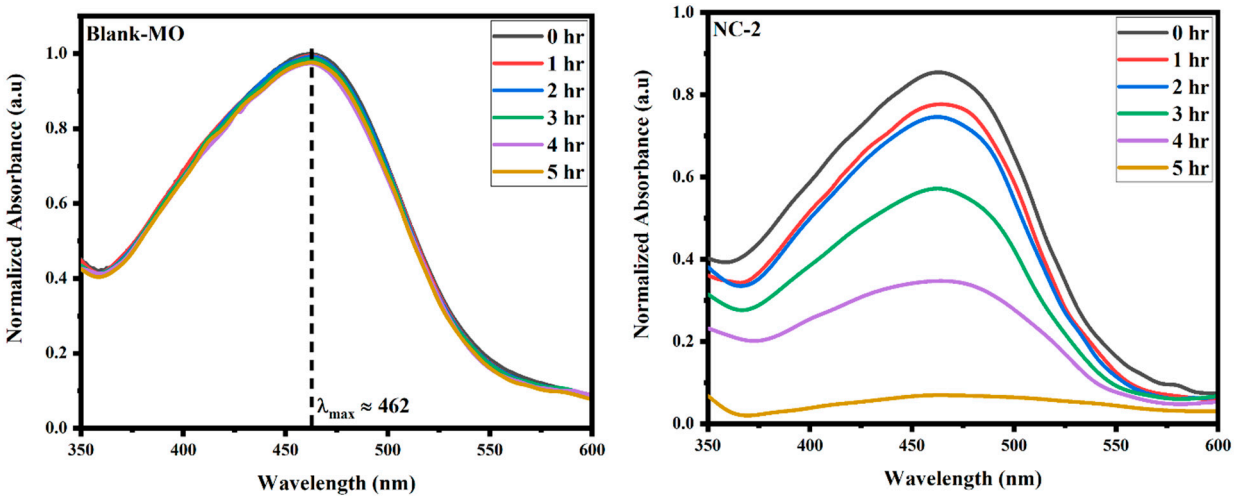

(**a**) (**b**)

Figure 6. UV/visible spectral information for (**a**) Blank and (**b**) NC-2 under illumination.

Photodegradation efficiency of all prepared catalysts against methyl orange was calculated by the formula:

$$\text{Percentage Efficiency} = [(A_o - A_t)/A_o] \times 100$$

where A_o is absorbance at time 0 min and A_t is absorbance after time "t" min of the photodegradation experiment. A_o and A_t were recorded at λ_{max} of the dye [51]. Figure 7 shows the comparison of the percentage efficiency of all prepared catalysts against methyl orange. The highest efficiency was calculated for NC-2, which is due to the optimum

constitution of Bi_2O_3 and $CoFe_2O_4$ (1:1) as well as the effective migration of exciton pairs in the type-II band configuration between the constituent materials, resulting in the suppression of charge recombination.

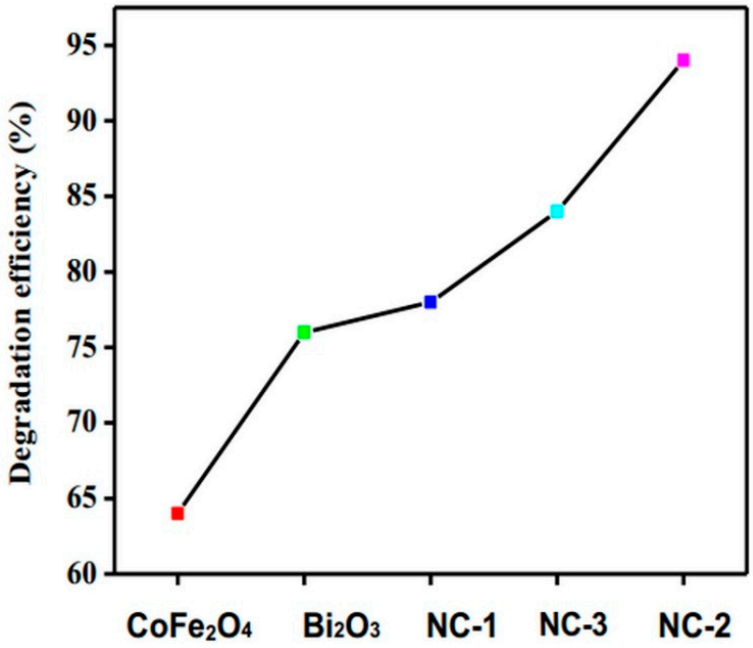

Figure 7. Comparison of percentage efficiency of all prepared photocatalysts for methyl orange degradation.

2.6. Proposed Photodegradation Scheme

According to the aforementioned results, a speculative photocatalytic mechanism based on bibliographic data is proposed in Figure 8 [39,52–54]. Under continuous light irradiation, electrons become excited from valence bands of $CoFe_2O_4$ and Bi_2O_3 to their conduction bands, meanwhile producing holes in their respective valence bands. As both the valence band and conduction band of the $CoFe_2O_4$ are lower in energy than those of Bi_2O_3, cobalt ferrite acts as a light energy trapper. Subsequently, these electrons and holes are rearranged and enriched into the conduction band of Bi_2O_3 and the valence band of $CoFe_2O_4$, respectively. A band-to-band transition bridge is established between Bi_2O_3 and cobalt ferrite in which the energy levels are mismatched between each other. Since the conduction band potential of $CoFe_2O_4$ is more negative than that of Bi_2O_3, excited electrons are constantly shifted to the conduction band of Bi_2O_3. Meanwhile, as the valence band of $CoFe_2O_4$ is less positive than that of the Bi_2O_3, holes in the VB of Bi_2O_3 will transfer continuously to the VB of cobalt ferrite. This synergism will reduce the cogent band gap, hinder electron hole recombination and will increase electron hole availabilities for photodegradation reactions, thus ensuring efficient photodegradation co-work of $Bi_2O_3/CoFe_2O_4$ nanocomposites.

These holes in the VB of cobalt ferrite will react to H_2O/OH^- and produce highly reactive $OH^\bullet$ radicals to start the process of degradation. Simultaneously, electrons gathered in the conduction band of Bi_2O_3 react with adsorbed oxygen and form oxidants such as superoxide ions. These active species such as $OH^\bullet$ and $O_2^{\bullet-}$ radicals react to degrade molecules of the dye into H_2O, CO_2 or other small molecular products. Chemical equations of this speculative photocatalytic mechanism based on bibliographic data are illustrated as:

$$CoFe_2O_4 + Bi_2O_3 + 2h\nu \rightarrow CoFe_2O_4\ (e^- + h^+) + Bi_2O_3\ (e^- + h^+) \quad (1)$$

$$CoFe_2O_4\ (e^- + h^+) + Bi_2O_3\ (e^- + h^+) \rightarrow CoFe_2O_4\ (2h^+) + Bi_2O_3\ (2e^-) \quad (2)$$

$$Bi_2O_3\ (2e^-) + 2O_2 \rightarrow 2O_2^{\bullet-} + Bi_2O_3 \quad (3)$$

$$CoFe_2O_4\ (2h^+) + 2OH^- \rightarrow CoFe_2O_4 + 2OH^\bullet \quad (4)$$

$$Dye + O_2^{\bullet -} + OH^\bullet \rightarrow CO_2 + H_2O + \text{other by-product} \quad (5)$$

The $Bi_2O_3/CoFe_2O_4$ heterojunction designed in this study is not similar to the type-I heterojunction structure. It is considered for the $Bi_2O_3/CoFe_2O_4$ that $CoFe_2O_4$ plays its role as the main photocatalyst, while the Bi_2O_3 works as a photosensitizer [14,55,56]. The VB edge of Bi_2O_3 is lower than that of $CoFe_2O_4$; hence, this system is a type-II heterojunction [57,58]. Since these heterojunctions are tightly bounded at the nanoscale, the hole transfers through the junction are efficacious. Furthermore, the $CoFe_2O_4$, working as the main photocatalyst, is found side-by-side in the $Bi_2O_3/CoFe_2O_4$ nanocomposite. Hence, formation of a heterojunction structure does not shield the active sites of catalysts.

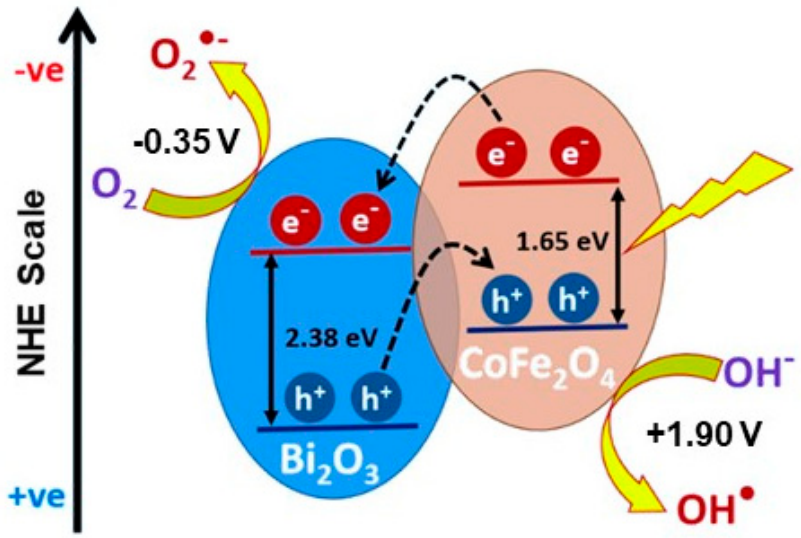

Figure 8. Schematic illustration of energy level alignment and photodegradation action of $Bi_2O_3/CoFe_2O_4$ nanocomposites.

3. Materials and Methods

All the materials, viz., bismuth (III) nitrate pentahydrate, cobalt chloride hexahydrate, ferric chloride hexahydrate, polyvinyl pyrrolidone (MW 40,000), sodium hydroxide, nitric acid and glycerol were purchased from Daejung, Korea and used without further purification. Ethanol and deionized water were used for washing and preparation of solutions. Various concentrations of precursor solution and conditions of reactions were explored for material synthesis based on reported methods. However, the following optimized methods proved to avoid agglomeration of individual products and composites.

3.1. Synthesis of Bi_2O_3 Nanoparticles

Bismuth nitrate pentahydrate (0.97 g) was dissolved in 10 mL of 1.12 M HNO_3 along with vigorous stirring in order to avoid hydrolyzation of Bi^{3+} ions. Subsequently, 0.072 g of polyvinylpyrrolidone (PVP) was added as surfactant into the above mixture and stirred by manual stirring for about 15–20 min. Later, 4 M NaOH solution was gradually added with constant stirring until the pH of the solution turned basic (pH = 11) and white precipitates appeared. After stirring for 10 min, the resultant suspension was placed into a Teflon-lined autoclave (KH100, Guangzhou Aolantec, China) at 90 °C for 1 h. The suspension was allowed to cool at room temperature and its white color turned to yellow. The resultant yellow precipitates were centrifuged in a centrifuge (Hermle, Germany) and washed with distilled water/ethanol several times. The resultant product was dried in a vacuum oven (Memmert, Germany) for 2 h at 80 °C. This furnished yellow, solid particles of bismuth oxide which were ground into a fine powder. This powder was further calcined at 400 °C for 4 h [42,43].

3.2. Synthesis of $CoFe_2O_4$ Nanoparticles

Magnetic cobalt ferrite nanoparticles were prepared via a simple, one-pot hydrothermal process. An aqueous solution containing 4 mmol $FeCl_3 \cdot 6H_2O$ was mixed with 0.078 M glycerol (surfactant) under constant stirring. Afterward, 2 mmol $CoCl_2 \cdot 6H_2O$ solution was added slowly into the above mixture to prepare a uniform solution. Highly alkaline conditions (pH = 13) of the reaction mixture were maintained by dropwise addition of 6 M NaOH solution. This resulted in a brownish-black precipitate mixture. Subsequently, the reaction mixture was transferred into a Teflon-lined autoclave and kept in an oven for 6 h at 200 °C. The resultant suspension was centrifuged and washed with distilled water several times. Later, the precipitates were dried at 100 °C for 6 h in a vacuum oven. The resultant cobalt ferrite product was ground into a powder [44,45].

3.3. Synthesis of $Bi_2O_3/CoFe_2O_4$ Nanocomposites

A physical method was opted for in order to prepare the nanocomposites. This involved simple, solid-state mixing of already synthesized bismuth oxide and cobalt ferrite nanoparticles, followed by 3 h grinding via pestle and mortar. Resultant mixtures were calcined at 400 °C for 4 h. Three nanocomposites with different proportions of $CoFe_2O_4$ and Bi_2O_3 were prepared (Table 4).

Table 4. Details of $Bi_2O_3/CoFe_2O_4$ nanocomposites.

	Wt.% of Bi_2O_3	**Wt.% of $CoFe_2O_4$**
NC-1	25	75
NC-2	50	50
NC-3	75	25

3.4. Degradation Experiment

Photodegradation studies were carried out against methyl orange dye to explore the photocatalytic properties of as-prepared nanocomposites. A 300 W xenon arc lamp was used as the light source for degradation studies and to irradiate beakers charged with dye stock solution and catalyst. A stock solution of 30 ppm methyl orange dye was prepared in distilled water. For each photodegradation run, 50 mL stock solution was poured into beakers and 10 mg of each prepared catalyst nanocomposite was added into these separately. These solutions were kept in the dark with constant stirring for 2 h to attain adsorption–desorption equilibrium. Afterward, samples were kept in a photoreactor chamber and light was shone on the system. After different predetermined intervals of time, 5 mL of each solution was stripped out and centrifuged for 5 min at 10,000 rpm to let the catalyst settle down. The solutions obtained were examined by UV–visible spectrophotometer (UV/Vis Lambda 365, Perkin Elmer, Akron, OH, USA) to ascertain the residual dye contents in the solution in order to study the photocatalytic activity and the level of methyl orange degradation [46,47].

4. Conclusions

$Bi_2O_3/CoFe_2O_4$ photocatalysts were successfully prepared by a facile agitation and the influence of different proportions of constituents was also investigated systematically. The results of XRD, SEM, EDX and UV–visible DRS spectroscopy have corroborated the synthesis of nanocomposites without any further chemical reaction or by-products, nor any change in morphology of the constituent chemicals. $Bi_2O_3/CoFe_2O_4$ heterojunctions have shown a high efficiency for decomposing organic dye under light irradiation as compared to both of the individual components. Furthermore, $Bi_2O_3/CoFe_2O_4$ induced mineralization by utilizing the electrons and the holes that were enriched in the conduction band of Bi_2O_3 and the valence band of $CoFe_2O_4$, respectively. The results suggested that $CoFe_2O_4$ acts as the main photocatalyst, while Bi_2O_3 works as a photosensitizer. The nanocomposite with 1:1 $Bi_2O_3/CoFe_2O_4$ composition showed the highest photodegradation efficiency, i.e.,

92% for the degradation of methyl orange dye. The superior photocatalytic performance of the nanocomposite may be credited to its type-II band configuration, which results in the suppression of charge recombination because Bi_2O_3 acts as an electron sink. As per our research, no prior study has been reported in the literature regarding the synthesis of a $Bi_2O_3/CoFe_2O_4$ nanocomposite and its dye degradation potential. Therefore, good photocatalytic degradation activities, demonstrated by these nanocomposites, for contaminated aqueous solutions make these materials a potent candidate to develop robust photocatalysts for practical applications in water decontamination technology. The $Bi_2O_3/CoFe_2O_4$ is environmentally friendly, the synthesis is simple, and, if it were scaled up, the manufacturing cost would be low. This also leaves scope for researchers to further explore its photocatalytic activities against other dye/drug pollutants and its water splitting potential.

Author Contributions: Conceptualization, A.B.N., A.M. and A.S.; methodology A.B.N., F.R. and S.A.; formal analysis, F.R. and A.S.; writing—original draft preparation A.B.N., A.S. and S.A.; writing—review and editing, A.M.; supervision, A.M. All authors have read and agreed to the published version of the manuscript.

Funding: This research received no external funding.

Acknowledgments: The authors are thankful to Institute of Environmental Sciences & Engineering, School of Chemical & Materials Engineering, U.S.–Pakistan Center for Advanced Studies in Energy of NUST and the National Centre for Physics of QAU for extending their technical support to this research work.

Conflicts of Interest: The authors declare no conflict of interest.

References

1. Gao, Q.; Xu, J.; Bu, X.-H. Recent advances about metal–organic frameworks in the removal of pollutants from wastewater. *Coord. Chem. Rev.* **2019**, *378*, 17–31. [CrossRef]
2. Chong, M.N.; Jin, B.; Chow, C.W.; Saint, C. Recent developments in photocatalytic water treatment technology: A review. *Water Res.* **2010**, *44*, 2997–3027. [CrossRef] [PubMed]
3. Mohammed, R.R. Removal of heavy metals from wastewater using black tea waste. *Arab. J. Sci. Eng.* **2012**, *37*, 1505–1520. [CrossRef]
4. Manaa, Z.; Chebli, D.; Bouguettoucha, A.; Atout, H.; Amrane, A. Low-Cost Photo-Fenton-Like Process for the Removal of Synthetic Dye in Aqueous Solution at Circumneutral pH. *Arab. J. Sci. Eng.* **2019**, *44*, 9859–9867. [CrossRef]
5. Dellamatrice, P.M.; Silva-Stenico, M.E.; de Moraes, L.A.B.; Fiore, M.F.; Monteiro, R.T.R. Degradation of textile dyes by cyanobacteria. *Braz. J. Microbiol.* **2017**, *48*, 25–31. [CrossRef] [PubMed]
6. Kooh, M.R.R.; Dahri, M.K.; Lim, L.B.; Lim, L.H. Batch adsorption studies on the removal of acid blue 25 from aqueous solution using Azolla pinnata and soya bean waste. *Arab. J. Sci. Eng.* **2016**, *41*, 2453–2464. [CrossRef]
7. Gupta, V.K.; Ali, I.; Saleh, T.A.; Nayak, A.; Agarwal, S. Chemical treatment technologies for waste-water recycling—An overview. *Rsc. Adv.* **2012**, *2*, 6380–6388. [CrossRef]
8. Esplugas, S.; Bila, D.M.; Krause, L.G.T.; Dezotti, M. Ozonation and advanced oxidation technologies to remove endocrine disrupting chemicals (EDCs) and pharmaceuticals and personal care products (PPCPs) in water effluents. *J. Hazard. Mater.* **2007**, *149*, 631–642. [CrossRef]
9. Moo-Young, H.K. Pulp and paper effluent management. *JSTOR* **2007**, *79*, 1733–1741. [CrossRef]
10. Maleš, L.; Fakin, D.; Bračič, M.; Gorgieva, S. Efficiency of Differently Processed Membranes Based on Cellulose as Cationic Dye Adsorbents. *Nanomaterials* **2020**, *10*, 642. [CrossRef]
11. Gogate, P.R.; Pandit, A.B. A review of imperative technologies for wastewater treatment II: Hybrid methods. *Adv. Environ. Res.* **2004**, *8*, 553–597. [CrossRef]
12. Rauwel, P.; Uhl, W.; Rauwel, E. *Editorial for the Special Issue on 'Application and Behavior of Nanomaterials in Water Treatment'*; Multidisciplinary Digital Publishing Institute: Basel, Switzerland, 2019.
13. Coleman, H.M.; Eggins, B.R.; Byrne, J.A.; Palmer, F.L.; King, E. Photocatalytic degradation of 17-β-oestradiol on immobilised TiO_2. *Appl. Catal. B Environ.* **2000**, *24*, L1–L5. [CrossRef]
14. Akpan, U.G.; Hameed, B.H. Parameters affecting the photocatalytic degradation of dyes using TiO_2-based photocatalysts: A review. *J. Hazard. Mater.* **2009**, *170*, 520–529. [CrossRef]
15. Chauhan, N.; Singh, V.; Kumar, S.; Dhiman, R. Influence of Nickel, Silver, and Sulphur Doping on the Photocatalytic Efficiency of Mesoporous ZnO Nanoparticles. *Arab. J. Sci. Eng.* **2020**, *45*, 249–259. [CrossRef]
16. Kabra, K.; Chaudhary, R.; Sawhney, R.L. Treatment of hazardous organic and inorganic compounds through aqueous-phase photocatalysis: A review. *Ind. Eng. Chem. Res.* **2004**, *43*, 7683–7696. [CrossRef]

17. Hoffmann, M.R.; Martin, S.T.; Choi, W.; Bahnemann, D.W. Environmental applications of semiconductor photocatalysis. *Chem. Rev.* **1995**, *95*, 69–96. [CrossRef]
18. Ismail, N.J.; Othman, M.H.D.; Kamaludin, R.; Esham, M.I.M.; Ali, N.A.; Rahman, M.A.; Jaafar, J.; Bakar, S.A. Characterization of Bauxite as a Potential Natural Photocatalyst for Photodegradation of Textile Dye. *Arab. J. Sci. Eng.* **2019**, *44*, 10031–10040. [CrossRef]
19. Khan, M.M.; Adil, S.F.; Al-Mayouf, A. *Metal Oxides as Photocatalysts*; Elsevier: Amsterdam, The Netherlands, 2015.
20. Zhou, H.; Qu, Y.; Zeid, T.; Duan, X. Towards highly efficient photocatalysts using semiconductor nanoarchitectures. *Energy Environ. Sci.* **2012**, *5*, 6732–6743. [CrossRef]
21. Saravanan, R.; Gupta, V.K.; Narayanan, V.; Stephen, A. Comparative study on photocatalytic activity of ZnO prepared by different methods. *J. Mol. Liq.* **2013**, *181*, 133–141. [CrossRef]
22. Khan, M.M.; Ansari, S.A.; Pradhan, D.; Ansari, M.O.; Lee, J.; Cho, M.H. Band gap engineered TiO_2 nanoparticles for visible light induced photoelectrochemical and photocatalytic studies. *J. Mater. Chem. A* **2014**, *2*, 637–644. [CrossRef]
23. Boudjemaa, A.; Popescu, I.; Juzsakova, T.; Kebir, M.; Helaili, N.; Bachari, K.; Marcu, I.C. M-Substituted (M=Co, Ni and Cu) Zinc Ferrite Photo-Catalysts for Hydrogen Production by Water Photo-Reduction. *Int. J. Hydrog. Energy* **2016**, *41*, 11108–11118. [CrossRef]
24. Deng, Y.; Zhao, X.; Luo, J.; Wang, Z.; Tang, J. Magnetic Recyclable $CoFe_2O_4$@ Ppy Prepared by in Situ Fenton Oxidization Polymerization with Advanced Photo-Fenton Performance. *RSC Adv. Tang* **2020**, *10*, 1858–1869. [CrossRef]
25. Dutta, V.; Sheetal, S.; Pankaj, R.; Ahmad, H.B.; Vinod, K.G.; Pardeep, J. Review on Augmentation in Photocatalytic Activity of $CoFe_2O_4$ Via Heterojunction Formation for Photocatalysis of Organic Pollutants in Water. *J. Saudi Chem. Soc. Singh* **2019**, *23*, 1119–1136.
26. Habibi, M.H.; Janan, J. Cobalt Ferrite Nano-Composite Coated on Glass by Doctor Blade Method for Photo-Catalytic Degradation of an Azo Textile Dye Reactive Red 4: Xrd, Fesem and Drs Investigations. *Spectrochim. Acta Part A Mol. Parhizkar Biomol. Spectrosc.* **2015**, *150*, 879–885. [CrossRef]
27. Sharma, R.; Kumar, V.; Bansal, S.; Singhal, S. Boosting the Catalytic Performance of Pristine $CoFe_2O_4$ with Yttrium (Y^{3+}) Inclusion in the Spinel Structure. *Mater. Res. Bull. Singhal* **2017**, *90*, 94–103. [CrossRef]
28. Devi, L.G.; Srinivas, M. Hydrothermal synthesis of reduced graphene oxide-CoFe2O4 heteroarchitecture for high visible light photocatalytic activity: Exploration of efficiency, stability and mechanistic pathways. *J. Environ. Chem. Eng.* **2017**, *5*, 3243–3255. [CrossRef]
29. Yamani, Z. Magnetic Properties and Photocatalytic Degradation Performance of MFe_2O_4 (M=Co, Ni)/Biocl Composites Catalysts under Uv Light Irradiation. *Arab. J. Sci. Eng.* **2018**, *43*, 383–388. [CrossRef]
30. Fan, H.; Pan, S.; Teng, X.; Ye, C.; Li, G.; Zhang, L. δ-Bi_2O_3 thin films prepared by reactive sputtering: Fabrication and characterization. *Thin Solid Film.* **2006**, *513*, 142–147. [CrossRef]
31. Shan, D.; Zhang, J.; Xue, H.-G.; Zhang, Y.-C.; Cosnier, S.; Ding, S.-N. Polycrystalline bismuth oxide films for development of amperometric biosensor for phenolic compounds. *Biosens. Bioelectron.* **2009**, *24*, 3671–3676. [CrossRef]
32. Shafi, K.V.; Gedanken, A.; Prozorov, R.; Balogh, J. Sonochemical preparation and size-dependent properties of nanostructured $CoFe_2O_4$ particles. *Chem. Mater.* **1998**, *10*, 3445–3450. [CrossRef]
33. Zi, Z.; Sun, Y.; Zhu, X.; Yang, Z.; Dai, J.; Song, W. Synthesis and magnetic properties of $CoFe_2O_4$ ferrite nanoparticles. *J. Magn. Magn. Mater.* **2009**, *321*, 1251–1255. [CrossRef]
34. Ullah, I.; Ali, S.; Hanif, M.A.; Shahid, S.A. Nanoscience for environmental remediation: A review. *Int. J. Chem. Biochem. Sci.* **2012**, *2*, 60–77.
35. Dong, F.; Guo, S.; Wang, H.; Li, X.; Wu, Z. Enhancement of the visible light photocatalytic activity of C-doped TiO_2 nanomaterials prepared by a green synthetic approach. *J. Phys. Chem. C* **2011**, *115*, 13285–13292. [CrossRef]
36. Narayana, R.L.; Matheswaran, M.; Aziz, A.A.; Saravanan, P. Photocatalytic decolourization of basic green dye by pure and Fe, Co doped TiO_2 under daylight illumination. *Desalination* **2011**, *269*, 249–253. [CrossRef]
37. Dippong, T.; Levei, E.A.; Deac, I.G.; Neag, E.; Cadar, O. Influence of Cu^{2+}, Ni^{2+}, and Zn^{2+} Ions Doping on the Structure, Morphology, and Magnetic Properties of Co-Ferrite Embedded in SiO_2 Matrix Obtained by an Innovative Sol-Gel Route. *Nanomaterials* **2020**, *10*, 580. [CrossRef] [PubMed]
38. Serpone, N.; Emeline, A. *Semiconductor Photocatalysis-Past, Present, and Future Outlook*; ACS Publications: Washington, DC, USA, 2012.
39. Chen, S.; Hu, Y.; Ji, L.; Jiang, X.; Fu, X. Preparation and characterization of direct Z-scheme photocatalyst $Bi_2O_3/NaNbO_3$ and its reaction mechanism. *Appl. Surf. Sci.* **2014**, *292*, 357–366. [CrossRef]
40. Kang, I.-C.; Zhang, Q.; Yin, S.; Sato, T.; Saito, F. Improvement in photocatalytic activity of TiO_2 under visible irradiation through addition of N-TiO_2. *Environ. Sci. Technol.* **2008**, *42*, 3622–3626. [CrossRef] [PubMed]
41. Bai, S.; Liu, H.; Sun, J.; Tian, Y.; Chen, S.; Song, J.; Luo, R.; Li, D.; Chen, A.; Liu, C.-C. Improvement of TiO2 photocatalytic properties under visible light by WO_3/TiO_2 and MoO_3/TiO_2 composites. *Appl. Surf. Sci.* **2015**, *338*, 61–68. [CrossRef]
42. Oudghiri-Hassani, H.; Rakass, S.; Al Wadaani, F.T.; Al-Ghamdi, K.J.; Omer, A.; Messali, M.; Abboudi, M. Synthesis, characterization and photocatalytic activity of α-Bi_2O_3 nanoparticles. *J. Taibah Univ. Sci.* **2015**, *9*, 508–512. [CrossRef]
43. Mallahi, M.; Shokuhfar, A.; Vaezi, M.; Esmaeilirad, A.; Mazinani, V. Synthesis and characterization of bismuth oxide nanoparticles via sol-gel method. *AJER* **2014**, *3*, 162–165.

44. Cote, L.J.; Teja, A.S.; Wilkinson, A.P.; Zhang, Z.J. Continuous hydrothermal synthesis of $CoFe_2O_4$ nanoparticles. *Fluid Phase Equilibria* **2003**, *210*, 307–317. [CrossRef]
45. Maaz, K.; Mumtaz, A.; Hasanain, S.; Ceylan, A. Synthesis and magnetic properties of cobalt ferrite ($CoFe_2O_4$) nanoparticles prepared by wet chemical route. *J. Magn. Magn. Mater.* **2007**, *308*, 289–295. [CrossRef]
46. Li, Y.; Li, X.; Li, J.; Yin, J. Photocatalytic degradation of methyl orange by TiO_2-coated activated carbon and kinetic study. *Water Res.* **2006**, *40*, 1119–1126. [CrossRef] [PubMed]
47. Wang, C.; Wang, X.; Xu, B.-Q.; Zhao, J.; Mai, B.; Sheng, G.; Fu, J. Enhanced photocatalytic performance of nanosized coupled ZnO/SnO_2 photocatalysts for methyl orange degradation. *J. Photochem. Photobiol. A Chem.* **2004**, *168*, 47–52. [CrossRef]
48. Mendelson, M.I. Average grain size in polycrystalline ceramics. *J. Am. Ceram. Soc.* **1969**, *52*, 443–446. [CrossRef]
49. Medernach, J.W.; Snyder, R.L. Powder diffraction patterns and structures of the bismuth oxides. *J. Am. Ceram. Soc.* **1978**, *61*, 494–497. [CrossRef]
50. Khan, M.S.; Ashiq, M.N.; Ehsan, M.F.; He, T.; Ijaz, S. Controlled synthesis of cobalt telluride superstructures for the visible light photo-conversion of carbon dioxide into methane. *Appl. Catal. A Gen.* **2014**, *487*, 202–209. [CrossRef]
51. Bera, K.K.; Majumdar, R.; Chakraborty, M.; Bhattacharya, S.K. Phase control synthesis of α, β and α/β Bi_2O_3 hetero-junction with enhanced and synergistic photocatalytic activity on degradation of toxic dye, Rhodamine-B under natural sunlight. *J. Hazard. Mater.* **2018**, *352*, 182–191. [CrossRef]
52. Cong, Y.; Zhang, J.; Chen, F.; Anpo, M.; He, D. Preparation, photocatalytic activity, and mechanism of nano-TiO_2 co-doped with nitrogen and iron (III). *J. Phys. Chem. C* **2007**, *111*, 10618–10623. [CrossRef]
53. Huang, S.; Xu, Y.; Xie, M.; Xu, H.; He, M.; Xia, J.; Huang, L.; Li, H. Synthesis of magnetic $CoFe_2O_4$/g-C_3N_4 composite and its enhancement of photocatalytic ability under visible-light. *Colloids Surf. A Physicochem. Eng. Asp.* **2015**, *478*, 71–80. [CrossRef]
54. Fu, J.; Tian, Y.; Chang, B.; Xi, F.; Dong, X. BiOBr–carbon nitride heterojunctions: Synthesis, enhanced activity and photocatalytic mechanism. *J. Mater. Chem.* **2012**, *22*, 21159–21166. [CrossRef]
55. Konstantinou, I.K.; Albanis, T.A. TiO_2-assisted photocatalytic degradation of azo dyes in aqueous solution: Kinetic and mechanistic investigations: A review. *Appl. Catal. B Environ.* **2004**, *49*, 1–14. [CrossRef]
56. Thiruvenkatachari, R.; Vigneswaran, S.; Moon, I.S. A review on UV/TiO_2 photocatalytic oxidation process (Journal Review). *Korean J. Chem. Eng.* **2008**, *25*, 64–72. [CrossRef]
57. He, G.; Ding, J.; Zhang, J.; Hao, Q.; Chen, H. One-step ball-milling preparation of highly photocatalytic active $CoFe_2O_4$–reduced graphene oxide heterojunctions for organic dye removal. *Ind. Eng. Chem. Res.* **2015**, *54*, 2862–2867. [CrossRef]
58. Kumar, A.; Kumar, A.; Sharma, G.; Ala'a, H.; Naushad, M.; Ghfar, A.A.; Guo, C.; Stadler, F.J. Biochar-templated g-C_3N_4/$Bi_2O_2CO_3$/$CoFe_2O_4$ nano-assembly for visible and solar assisted photo-degradation of paraquat, nitrophenol reduction and CO_2 conversion. *Chem. Eng. J.* **2018**, *339*, 393–410. [CrossRef]